Electronic Supplementary Material (ESI) for Physical Chemistry Chemical Physics.

Supplementary materials: Thermodynamics of amyloid fibril formation from chemical depolymerization

Nicola Vettore and Alexander K. Buell

Contents

Supplementary results

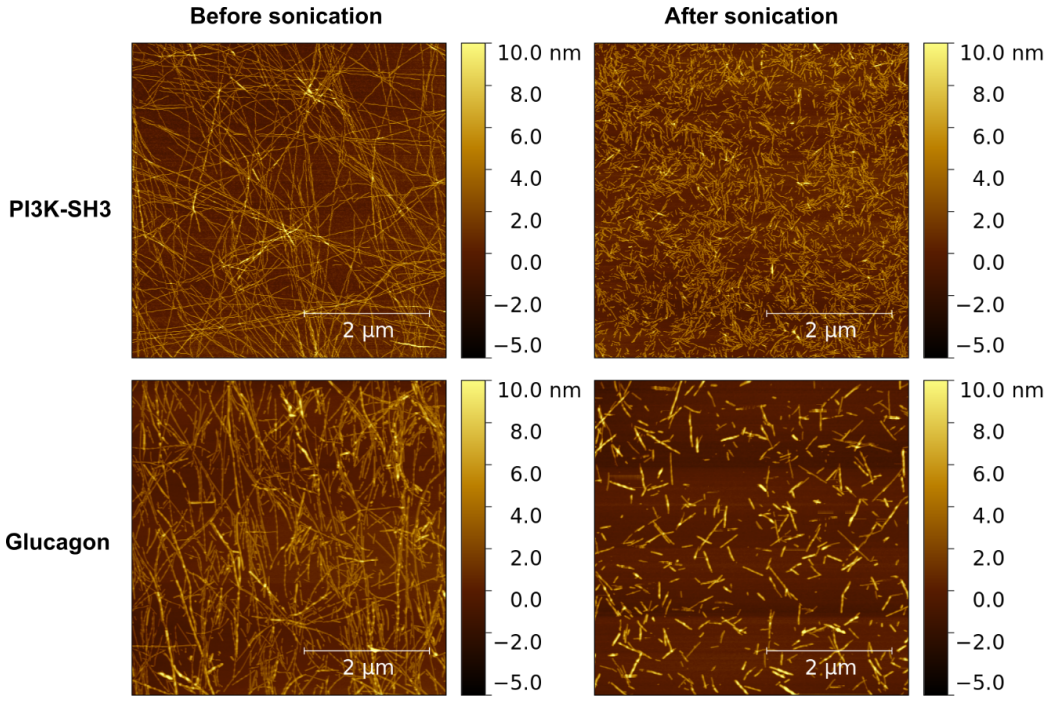

Figure 1: AFM images of PI3K-SH3 and glucagon fibrils, before and after sonication. See experimental methods section in main manuscript for details on the sonication and AFM imaging protocols.

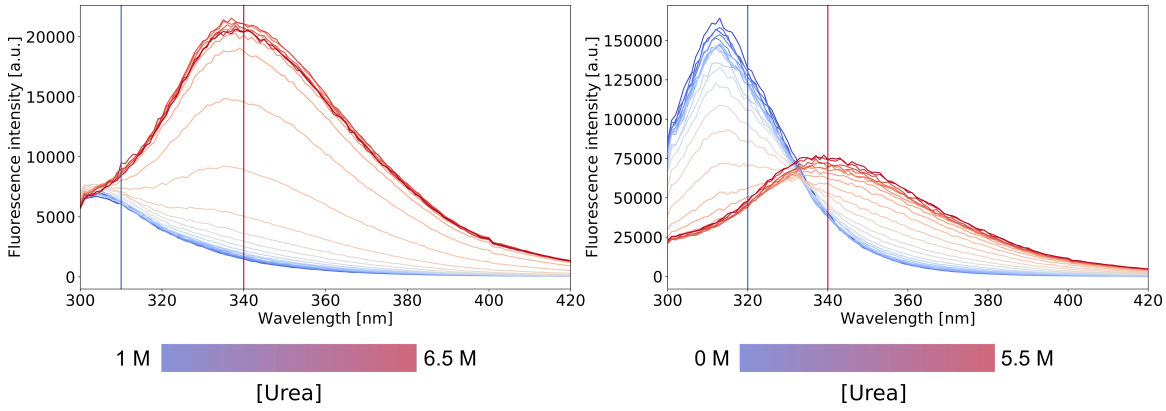

Figure 2: Intrinsic fluorescence spectra of PI3K-SH3 (left) and glucagon (right) at various denaturant concentrations. The fluorescence intensity ratios at the indicated wavelengths were analysed.

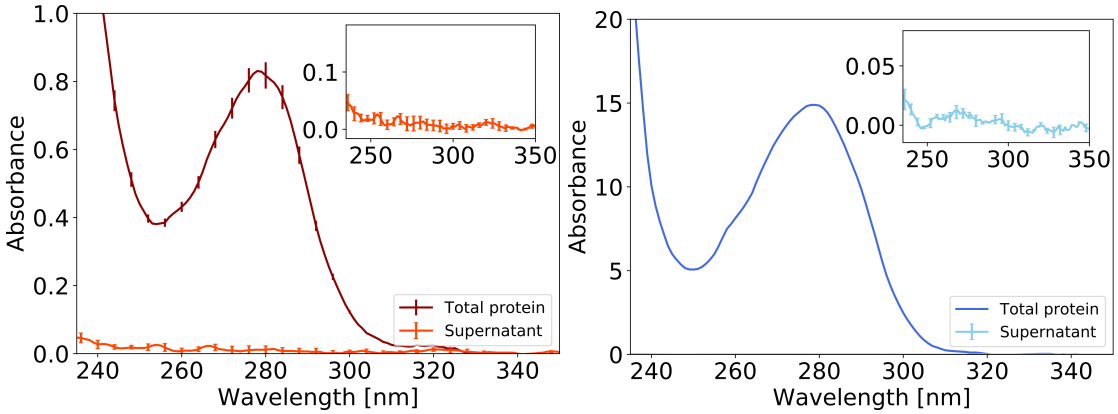

Figure 3: Quantification of soluble protein in supernatant before and after fibrillation, using absorbance spectroscopy. Left: PI3K-SH3; Right: glucagon. The errorbars represent the standard deviation on a sample size of n = 3. Details on the protocol of centrifugation can be found in the experimental methods section in the main manuscript. It can be seen from these results that the fibril formation reaction is near-complete and that the protein concentration in the supernatant is too low to be reliably measurable, illustrating the need to destabilise the fibrils with chemical denaturants.

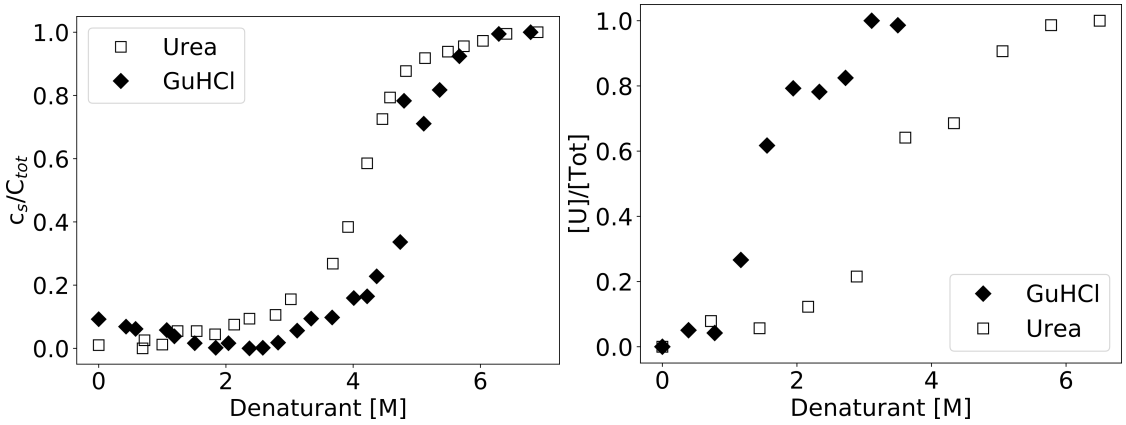

Figure 4: Comparison of urea and GndHCl depolymerization of SH3 fibrils and monomer at a total protein concentration of 50µM. Left panel: amyloid fibrils; Right panel: monomers.

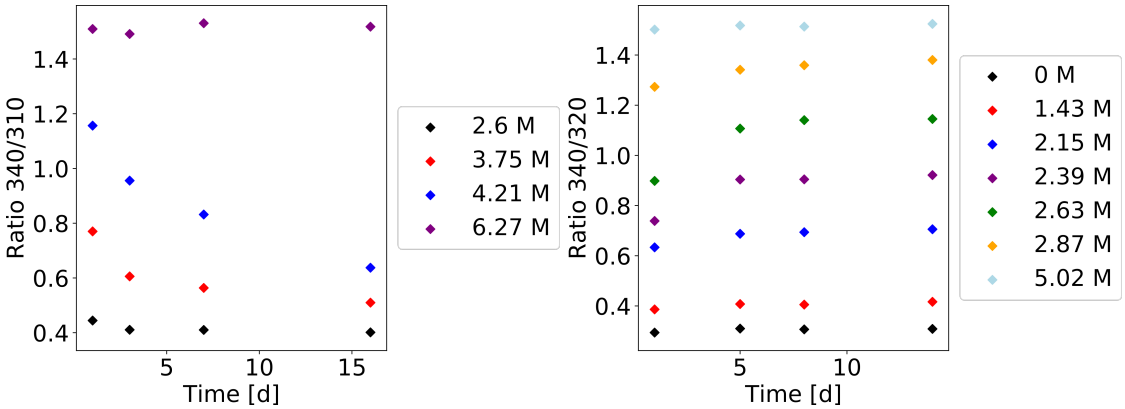

Figure 5: Time course of the fluorescence signal (expressed as intensity ratios at two wavelengths) of fibril samples with different urea molarities in order to monitor the time required for equilibration. Left: PI3K-SH3; Right: glucagon.

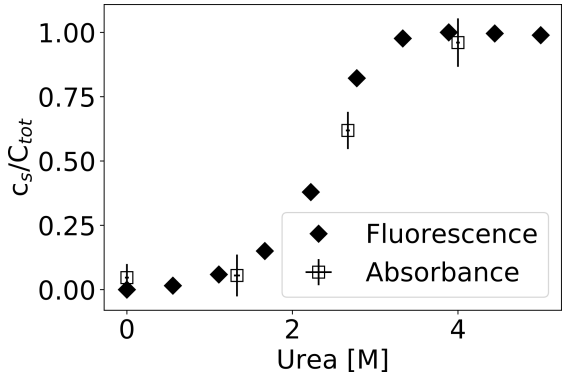

Figure 6: Direct comparison between absorbance (after centrifugation) and intrinsic fluorescence (intensity ratio 340/320 nm) data of urea depolymerization of glucagon amyloid fibrils. The errorbars represent the standard deviation on a sample size of n = 3.

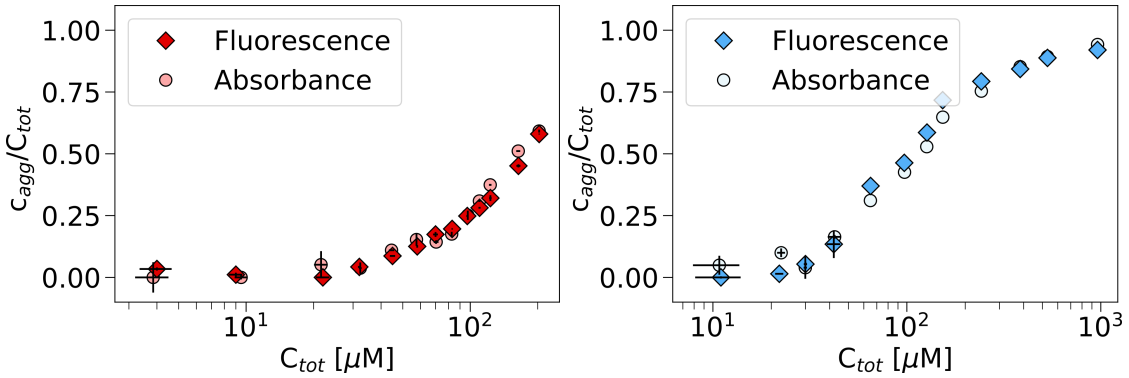

Figure 7: The degree of aggregation as a function of the total protein concentration for a given denaturant concentration. Data obtained from intrinsic fluorescence and direct quantification of soluble protein from supernatant absorbance are compared. In the fluorescence measurements the intensity ratios at 340/310 nm (PI3K-SH3) and 340/320 nm (glucagon) are monitored. Left panel: PI3K-SH3 amyloid fibrils equilibrated in 4 M Urea. Right panel: glucagon amyloid fibrils equilibrated in 3 M Urea.

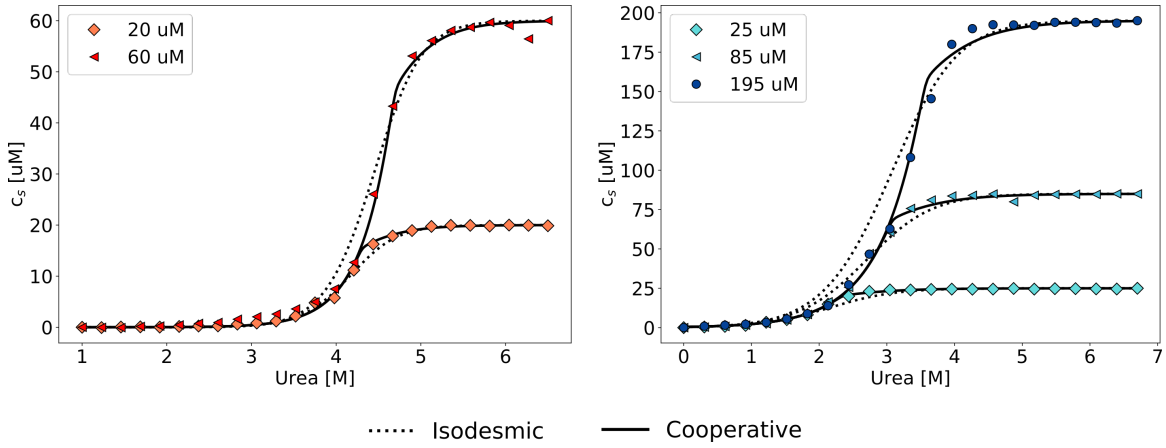

Figure 8: This is the same data set of chemical depolymerisation of PI3K-SH3 (left) and glucagon (right) as shown in Figures 1 and 2 of the main manuscript, but without normalising by the total protein concentration.

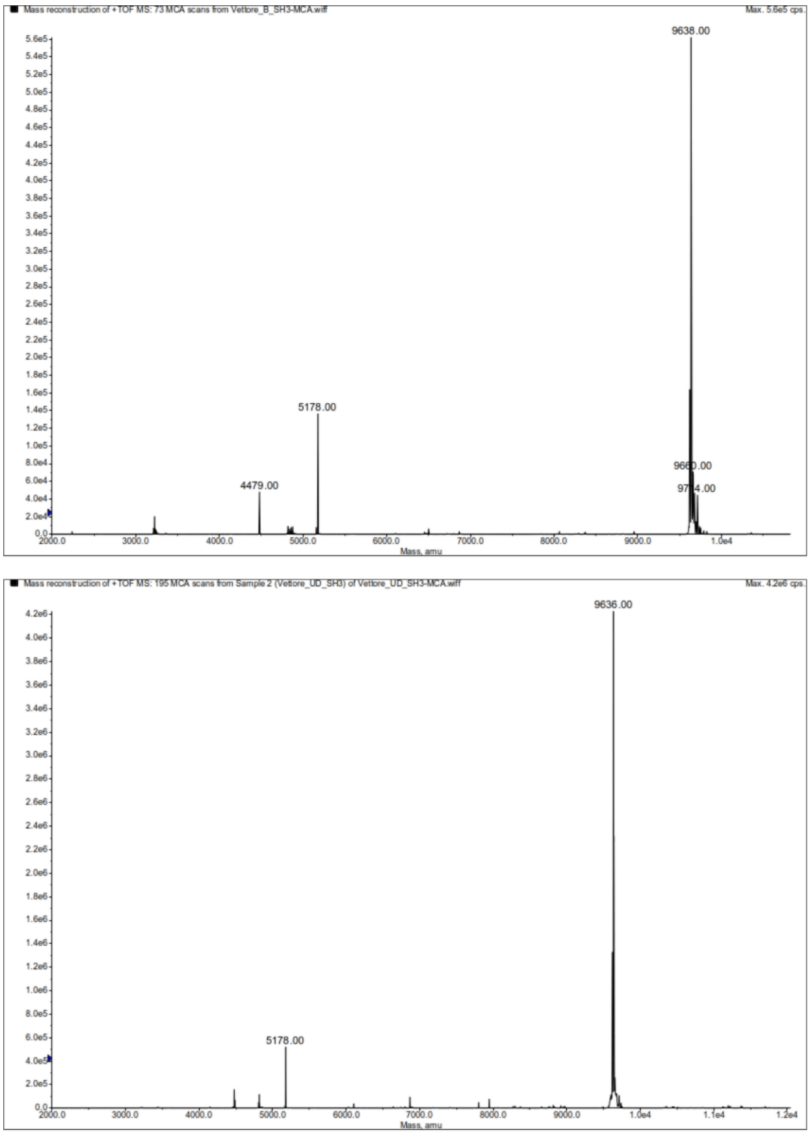

Figure 9: Mass spectra of PI3K-SH3 to probe carbamydation. PI3K-SH3 monomers were incubated for 9 days at room temperature in both buffer, 10 mM Glycine HCl pH 2 (top), and 6M Urea in buffer (bottom), at a final concentration of 100 μM. Afterwards, the sample containing urea was extensively dialysed against buffer to remove the urea. Both samples were then analysed by ESI-MS to check for possible carbamylation of the basic moieties of the protein. A small amount of fragmented protein (at position 39, peaks at 5178 Da and 4479 Da) is present in both samples and likely stems from the production.

Models for data analysis

Within the theoretical framework of the linear polymerization model we can describe the thermodynamics of formation of a linear polymer, such as an amyloid fibril, as a series of equilibria:

$$\begin{aligned}
\mathrm{M} + \mathrm{M} &\underset{\mathrm{k_{-2}}}{\overset{\mathrm{k_2}}{\rightleftharpoons}} \mathrm{M_2} \\
\mathrm{M_2} + \mathrm{M} &\underset{\mathrm{k_{-3}}}{\overset{\mathrm{k_3}}{\rightleftharpoons}} \mathrm{M_3} \\
\mathrm{M_3} + \mathrm{M} &\underset{\mathrm{k_{-4}}}{\overset{\mathrm{k_4}}{\rightleftharpoons}} \mathrm{M_4} \\
&\vdots \\
\mathrm{M}_{n-1} + \mathrm{M} &\underset{\mathrm{k_{-n}}}{\overset{\mathrm{k_n}}{\rightleftharpoons}} \mathrm{M}_n \\
&\vdots \\
\mathrm{M}_{i-1} + \mathrm{M} &\underset{\mathrm{k_{-i}}}{\overset{\mathrm{k_i}}{\rightleftharpoons}} \mathrm{M}_i
\end{aligned} \tag{1}$$

Each of these reactions is defined by an equilibrium constant which is defined as:

$$\mathrm{K}_i = \mathrm{k}_i/\mathrm{k}_{-i} = \frac{[\mathrm{M}_i]}{[\mathrm{M}_{i-1}][\mathrm{M}]} \tag{2}$$

Every $\mathrm{K_i}$ is then related to a free energy change, $\Delta \mathrm{G_i}^0$, by the relation:

$$\Delta \mathrm{G}_i^0 = -\mathrm{RT} \ln \mathrm{K_i} \tag{3}$$

The description of any real supra-molecular polymer system can then be based on this series of reactions by assuming certain relations between the different equilibrium constants, as will be shown in the following.

Isodesmic model

In the simplest form of the linear polymerization model, the so-called isodesmic model, it is assumed that the equilibrium constants $\mathrm{K_i}$ are equal for all the interactions. This means that the dimerization reaction will be associated with the same change in free energy as the interaction between a monomer and a polymer of length i. This simplicity allows to obtain an analytical solution that relates the monomer concentration at equilibrium to the total concentration of in the following way:

$$\mathrm{K}_e[\mathrm{M}] = 1 + \frac{1}{2\,\mathrm{K}_e[\mathrm{M}]_{\mathrm{tot}}} - \sqrt{\frac{1}{\mathrm{K_e}[\mathrm{M}]_{\mathrm{tot}}} + \frac{1}{4(\mathrm{K_e}[\mathrm{M}]_{\mathrm{tot}})^2}} \tag{4}$$

		Fit m [KJ mol^{-2}] as:				
		Local		Global		
Fit ΔG^0 [KJ mol^{-1}] as:	Local	-64.7	9.5	-70.0	10.1	20 µM
		-71.1	10.8	-67.7		60 µM
	Global	-66.8	10.0	-66.5	9.9	20 µM
			9.9			60 µM

Table 1: Parameters obtained from fits of the PI3K-SH3 amyloid fibril depolymerisation by using the isodesmic model. The table summarises the results from all combinations of global and local fits of the parameters $\Delta G^0$and m.

where K_e is the equilibrium constant that defines all the interactions between monomers and the other species in solutions, and $[M]_{tot}$ is the total concentration of the sample. This equation therefore describes the evolution of the concentration of monomeric protein, [M], as a function of total concentration. It is clear from this expression that the monomer concentration in an isodesmic system only asymtotically approaches a constant value, the so-called critical concentration.

In fibril depolymerization experiments where the concentration of denaturant, [D], is varied at constant $[M]_{tot}$, $K_e([D])$, is the independent variable. The two following relations can therefore be defined, in direct analogy to the linear free energy relationships in protein folding [1]:

$$K_e([D]) = \exp\left(-\frac{\Delta G([D])}{RT}\right) \tag{5}$$

$$\Delta G([D]) = {\Delta G_0}^{Buff} + m[D] \tag{6}$$

where ${\Delta G_0}^{Buff}$ is the free energy in the absence of denaturant. By introducing these terms in the equation 4, we can describe the depolymerisation curve as a function of the denaturant concentration as follows:

$$f_s = \frac{[M]}{[M]_{tot}} = \frac{2\,[M]_{tot}\exp\left(-\frac{\Delta G+m[D]}{RT}\right) + 1 - \sqrt{4[M]_{tot}\exp\left(-\frac{\Delta G+m[D]}{RT}\right) + 1}}{2\,[M]_{tot}^2\exp\left(-\frac{\Delta G+m[D]}{RT}\right)^2} \tag{7}$$

The dependence of the depolymerization profile on the total concentration allows to test the applicability of this theoretical framework to the system under study by globally fitting data at different protein concentrations, $[M]_{tot}$. In addition to testing the model, this procedure that we have employed in the present study, allows also to extract more robust thermodynamic parameters. Tables 1 and 2 below summarise the results of the possible combinations of glocal and local fits of the data shown in Figure 1 and 2 of the main manuscript.

Experimental data of amyloid fibril depolymerization by chemical denaturants has so far only been analyzed in the framework of this simplest model [2–4]. In the present study, however, we find that the isodesmic model is not able to quantitatively describe the ensemble of depolymerization curves

		Fit m [KJ mol^{-2}] as:				
		Local		Global		
Fit ΔG^0 [KJ mol^{-1}] as:	Local	-36.7	6.0	-35.7	5.7	25 µM
		-38.8	6.3	-37.2		85 µM
		-42.2	6.9	-38.2		195 µM
	Global	-36.9	6.1	-36.7	5.5	25 µM
			5.7			85 µM
			6.3			195 µM

Table 2: Parameters obtained from fits of the glucagon amyloid fibril depolymerisation by using the isodesmic model. The table summarises the results from all combinations of global and local fits of the parameters $\Delta G^0$and m.

at different protein concentrations. Furthermore, from a conceptual point of view, the isodesmic model is not a good description of a nucleated polymerization. Several simple extensions of the isodesmic model have therefore been introduced, all based on the idea that the equilibrium constant is size-dependent.

Helical and cooperative polymerization models

In their studies of actin, Oosawa and co-workers noticed that the polymerization behaviour of this protein was not compatible with the isodesmic model and as a consequence introduced the helical polymerization model[5,6]. In this model, a transition between the linear form of a trimer and a helical form is energetically unfavourable, due to elastic energy of deformation, but the addition of a monomer to the helical form is energetically more favorable than addition to the linear form, due to the larger number of inter-molecular contacts. The relevant equilibrium concentrations can be described as follows:

$$\begin{aligned}
&[\mathrm{M}_{3h}] = \gamma[\mathrm{M}_3] = \gamma \mathrm{K}^{-1}(\mathrm{K}[\mathrm{M}])^3 \\
&[\mathrm{M}_{4h}] = \mathrm{K}_h\,[\mathrm{M}_{3h}]\,[\mathrm{M}] = \gamma \mathrm{K}^{-1}\mathrm{K}^3\,\mathrm{K}_h\,[\mathrm{M}]^4 \\
&\quad .... \\
&[\mathrm{M}_{\mathrm{ih}}] = \mathrm{K}_h\,[\mathrm{M}_{(i-1)h}]\,[\mathrm{M}] = \gamma(\mathrm{K}/\mathrm{K}_h)^2\,{\mathrm{K}_h}^{-1}\,(\mathrm{K}_h\,[\mathrm{M}])^i = \sigma {\mathrm{K}_h}^{-1}\,(\mathrm{K}_h\,[\mathrm{M}])^i
\end{aligned} \tag{8}$$

where $\sigma = \gamma(K/K_h)^2$, with K the equilibrium constant of addition to a linear polymer, K_h the equilibrium constant for addition to a helical polymer and $\gamma < 1$ the unfavorable Boltzmann factor for mechanical deformation of the linear into a helical polymer. Usually, $\sigma \ll 1$ and therefore the system displays nucleation behaviour. It can be shown[6] that the total protein concentration in such a helically polymerizing system can be written as

$$[M]_{tot} = \frac{[M]}{(1-K[M])^2} + \frac{\sigma[M]}{(1-K_h[M])^2} - \sigma[M] - 2\sigma K_h[M] \tag{9}$$

which, for $\sigma \ll 1$ and $K < K_h$ can be simplified to

$$[M]_{tot} = [M] + \frac{\sigma[M]}{(1 - K_h[M])^2} \tag{10}$$

which predicts a well-defined critical concentration $[M_c] = K_h^{-1}$. The helical polymerization model in this form is elegant and well adapted to account for the specific structural features of actin filaments. It is, however, not the simplest extension of the isodesmic model. We chose to analyze our data on the chemical depolymerization of amyloid fibrils with an even simpler, and somewhat more general model, the so-called cooperative linear polymerization model [7,8]. This model introduces the assumption of a minimal unit of the polymer, called nucleus, the energetics of formation of which differs from that of elongation according to the following relation:

$$\mathrm{K}_n = \sigma \mathrm{K}_e \tag{11}$$

Note that the definition of σ is different than in the helical model. In this model, all reactions between a monomer and species up to n-mers (where n is the nucleus size) are described by the equilibrium constant $\mathrm{K_n}$, while the interactions between monomers and species with a higher number of monomers than n follow the equilibrium dictated by the constant $\mathrm{K_e}$. A detailed description of this model can be found in the review from Zhao and Moore [7]. Here we limit ourselves to a discussion of its application to analyze data of amyloid fibril thermodynamics.

Introducing the dimensionless concentrations $\mathrm{x_{tot}}=\mathrm{K_e[M]_{tot}}$ and $\mathrm{x}=\mathrm{K_e[M]}$, the relation between the two is described by the following equation formulated by Korevaar et al. [9]:

$$\mathrm{x_{tot}} = \sigma^{-1}\left(\frac{(\sigma \mathrm{x})^{n+1}(\mathrm{n}\sigma \mathrm{x} - n - 1)}{(\sigma \mathrm{x} - 1)^2} + \frac{\sigma \mathrm{x}}{(\sigma \mathrm{x} - 1)^2}\right) - \sigma^{n-1}\left(\frac{\mathrm{x}^{n+1}(\mathrm{nx} - n - 1)}{(\mathrm{x}\text{-}1)^2}\right) \tag{12}$$

This equation is solved numerically through the use of the *least_square* module of the *scipy.optimize* python library. In order to fit experimental data from a concentration series (see e.g. Figure 3 of the main manuscript), the solution of this equation for multiple $\mathrm{x_{tot}}$ is fitted using $[\mathrm{M}]_{\mathrm{tot}}$ as the independent variable and $\mathrm{K_e}$ as an open parameter (using the relation $\mathrm{x_{tot}}=\mathrm{K_e}[\mathrm{M}]_{\mathrm{tot}}$).

The fitting procedure for a depolymerization experiment, whereby the denaturant concentration is varied requires instead a different approach. The independent variable is [D], while $[\mathrm{M}]_{\mathrm{tot}}$ is kept constant and $\mathrm{K_e}$ is described in terms of $\mathrm{K}_e([\mathrm{D}]) = \exp\left(-(\Delta \mathrm{G_0}^{\mathrm{Buff}} + \mathrm{m[D]})/(\mathrm{RT})\right)$ with $\Delta \mathrm{G_0}^{\mathrm{Buff}}$, m and σ as fitting parameters, whereas n is kept constant for each given run.

Tables 3 and 4 below show the results of a systematic variation of the parameter n. We have performed fits for two types of models, which we call osaa and osam. The former (osaa, oligomers same as aggregates) corresponds to the scenario whereby the oligomers up to size n have the same fluorescence properties as the larger aggregates, whereas the latter (osam, oligomers same as monomers) corresponds to the scenario whereby all species up to size n have the same fluorescence properties as the monomer. It can be seen that the cooperative model, for all choices of n, provides a much better description of the concentration dependent depolymerization experiments than the isodesmic model. The fit parameters and fit quality are relatively insensitive to the exact choice of n, however, for both proteins the best results are achieved for small values of n of approximately 4-5. We have used n = 5 for the analysis of the influence of changes in salt concentration on the stability of the aggregates, see below. Regarding the choice of model (osam vs. osaa), we conclude that the osaa is not only structurally more plausible (due to the disordered nature of the monomers of both PI3K-SH3 [10] and glucagon [11] under these conditions, it can be expected that the monomer will have a distinct spectroscopic signature from any oligomeric species, which are likely to be more compact,

with solvent-protected Trp), but also yields lower values for σ. Smaller σ values correspond to a more distinct thermodynamic stability of small (<n) vs. large (>n) species, which we think is more plausible than σ value closer to unity.
We would like to stress here that n should not be regarded as a critical nucleus size. The values for $\Delta G^0$and σ we obtain from our fits suggest that also species below the size n are thermodynamically favourable (negative free energy of monomer attachment), albeit less so compared to monomer attachment to a species larger than n. In the framework of classical nucleation theory, the nucleus is considered a thermodynamically unstable species, i.e. the free energy of addition of a monomer to a species smaller than n is positive [12]. Our results suggest that the formation of small oligomeric species from amyloid proteins is thermodynamically favourable. However, it is still possible to explain the slow nucleation of amyloid fibrils, namely through the assumption of high free energy barriers for nucleation, as has been observed for example for the amyloid β-peptide [13]. When starting an aggregation experiment with freshly prepared monomeric protein, the establishment of the equilibrium distribution of small oligomers depends on the energy barriers rather than the thermodynamics of oligomer formation.

n	signal	ΔG^0[KJ/mol]	m [KJ/mol^2]	σ	R^2
isodesmic		-66.9	10	NaN	99.6
1	osaa	-67.9	10	NaN	99.6
	osam	-67.1	9.3	NaN	99.7
2	osaa	-59.2	7.6	0.110	99.8
	osam	-60.3	7.8	0.229	99.8
3	osaa	-58.5	7.3	0.139	99.8
	osam	-62.0	7.8	0.506	99.8
4	osaa	-57.7	7.1	0.132	99.8
	osam	-63.3	7.8	0.640	99.8
5	osaa	-57.1	6.9	0.121	99.8
	osam	-64.3	7.9	0.715	99.8
8	osaa	-57.0	6.8	0.113	99.8
	osam	-66.3	7.9	0.821	99.7
10	osaa	-56.9	6.8	0.113	99.8
	osam	-67.3	7.9	0.860	99.7
20	osaa	-63.9	8.6	0.285	99.6
	osam	-70.5	7.8	0.930	99.7
40	osaa	-63.9	8.6	0.285	99.6
	osam	-73.7	7.8	0.962	99.7

Table 3: Fitting parameters ΔG^0, m and σ from a systematic variation of n, in the framework of the two models osaa and osam (see text for details) for PI3K-SH3.

n	signal	ΔG^0[KJ/mol]	m [KJ/mol^2]	σ	R^2
isodesmic		-36.7	5.5	NaN	98.6
1	osaa	-37.4	5.7	NaN	98.6
	osam	-37.4	5.3	NaN	99.0
2	osaa	-36.0	4.2	0.030	99.8
	osam	-36.2	4.2	0.041	99.8
3	osaa	-36.2	4.1	0.084	99.8
	osam	-37.0	4.2	0.212	99.8
4	osaa	-36.2	4.1	0.097	99.8
	osam	-37.9	4.2	0.350	99.8
5	osaa	-36.3	4.1	0.102	99.7
	osam	-38.7	4.2	0.44	99.8
8	osaa	-36.5	4.2	0.115	99.7
	osam	-40.4	4.2	0.620	99.8
10	osaa	-36.5	4.2	0.115	99.7
	osam	-41.3	4.2	0.682	99.8
20	osaa	-36.5	4.2	0.115	99.7
	osam	-44.4	4.2	0.833	99.8
40	osaa	-36.5	4.2	0.115	99.7
	osam	-47.6	4.2	0.910	99.8

Table 4: Fitting parameters ΔG^0, m and σ from a systematic variation of n, in the framework of the two models osaa and osam (see text for details) for glucagon.

Electrostatic contribution to amyloid fibril stability

The basic assumption of the approach we present here is that the dependence of the rates and equilibria of molecular processes in aqueous solution on the salt concentration (or, more precisely, on the ionic strength) of the solution informs about the importance of electrostatic interactions in these processes and states. Conceptually, this approach is rooted in the work of Debye and Hückel, who presented a theory of electrostatic interactions in dilute salt solutions[14]. Here we follow and extend a treatment that we have presented previously in the context of the ionic strength dependence of amyloid fibril elongation rates[15]. The rate of amyloid fibril growth, R, can be written as $R = k_e[M][P]$, where k_e is the rate constant of elongation, [M] the monomer concentration and [P] the concentration of fibril ends. We have discussed previously[15,16] that k_e can be written as $k_e = \Gamma e^{-\frac{\Delta G^{\ddagger}}{RT}}$, whereby Γ is a diffusive pre-factor and $\Delta G^{\ddagger}$ is the free energy barrier for fibril elongation. An important point to mention here is while the process of incorporation of a monomer into a fibril end can involve the sequential crossing of multiple barriers, it is the highest barrier only that determines the kinetics[16,17]. This free energy barrier can be split into a non-electrostatic part ($\Delta G^{\ddagger}_{ne}$, breakage of H-bonds and other non-covalent interactions, hydrophobic effect, etc.[18]) and an electrostatic part ($\Delta G^{\ddagger}_{e}$). We postulate that the electrostatic contribution to $\Delta G^{\ddagger}$ can be written as a screened Coulomb potential[15,19]:

$$\Delta G^{\ddagger} = \Delta G^{\ddagger}_{ne} + \Delta G^{\ddagger}_{e} = \Delta G^{\ddagger}_{ne} + \frac{N_A z_M z_F e^2}{4\pi\epsilon_0\epsilon_r r^{\ddagger}} e^{-\kappa r^{\ddagger}} \tag{13}$$

where free energies are given in J/mol. Here, z_M and z_F denote the effective charges of the monomer and the fibril end, respectively, that lead to the electrostatic repulsion in the transition state. $\kappa = \sqrt{\frac{2000e^2 I N_A}{\epsilon_0\epsilon_r k_B T}}$ is the inverse Debye length and $r^{\ddagger}$ corresponds to the average centre of mass distance between the monomer and the fibril end in the transition state ensemble[15,16,18]. For $\kappa r^{\ddagger} < 1$, we can linearize this expression, by using $e^{-x} \approx 1 - x$ for small x:

$$\Delta G^{\ddagger} = \Delta G^{\ddagger}_{ne} + \frac{N_A z_M z_F e^2}{4\pi\epsilon_0\epsilon_r r^{\ddagger}} - \frac{N_A z_M z_F e^2 \kappa}{4\pi\epsilon_0\epsilon_r} \tag{14}$$

In this expression, only κ depends explicitly on the ionic strength; therefore, if we derive the logarithm of the fibril elongation rate with respect to the square root of the ionic strength, we obtain:

$$\frac{d\log R}{d\sqrt{I}} = \frac{N_A z_M z_F e^2}{4\pi\epsilon_0\epsilon_r RT}\frac{d\kappa}{d\sqrt{I}} = \frac{N_A z_M z_F e^2}{4\pi\epsilon_0\epsilon_r RT}\sqrt{\frac{2000e^2 N_A}{\epsilon_0\epsilon_r k_B T}} = A z_M z_F \tag{15}$$

We see, therefore, that the slope of a plot of the logarithm of the fibril elongation rate against the square root of the ionic strength is proportional to the product of the effective charges on the monomer and fibril end that are relevant for the interaction in the transition state of fibril elongation[15].

We next focus on the equilibrium constant for fibril elongation, which is related to the free energy change associated with the addition of one mole of monomer to fibril ends according to equation (3), $\Delta G^0 = -RT\ln K_e$. Again, we can divide ΔG^0 into a non-electrostatic contribution and an electrostatic contribution:

$$\Delta G^0 = \Delta G^0_{ne} + \Delta G^0_{e} = \Delta G^0_{ne} + \frac{N_A z'_M z'_F e^2}{4\pi\epsilon_0\epsilon_r r^{eq}} e^{-\kappa r^{eq}} \tag{16}$$

This expression is analogous to equation 13, except for the substitution of the ‡ ('double dagger') superscript (notation for transition state quantities) by the superscript 'eq'. Here, r^{eq} denotes the

Ionic strength $[\sqrt{M}]$	ΔG^0[KJ/mol] m glob. fit	ΔG^0[KJ/mol] m fixed
0.17	-35.2	-36.8
0.22	-37.3	-39.1
0.28	-38.2	-40.6
0.32	-39.5	-42.3
0.36	-40.1	-42.9

Table 5: Glucagon amyloid fibril stabilities as a function of salt concentration. In the first column, sigma is kept constant at 0.064, n is kept constant at 5 and m is globally fitted among the whole dataset. In the second column, m is also fixed as well at 4400 KJ/mol, the value determined previously from the fit of the data set in the absence of salt.

Ionic strength $[\sqrt{M}]$	ΔG^0[KJ/mol] m glob. fit	ΔG^0[KJ/mol] m fixed
0.17	-52.0	-56.0
0.18	-54.2	-59.0
0.19	-55.1	-59.9
0.22	-56.3	-61.2

Table 6: PI3K-SH3 amyloid fibril stabilities as a function of salt concentration. In the first column, sigma is kept constant at 0.121, n is kept constant at 5 and m is globally fitted among the whole dataset. In the second column, m is also fixed as well at 6900 KJ/mol, the value determined previously from the fit of the data set in the absence of salt.

center of mass distance of the last incorporated monomer from the previous fibril end, i.e. the center of mass of the second to last incorporated monomer. The effective charges have been primed in order to express the idea that the effective charges acting in the transition state ensemble and in the final state can be different. A rearrangement of this expression analogous to the one outlined for the kinetic expression above leads to:

$$\frac{d\log K_e}{d\sqrt{I}} = \frac{N_A z'_M z'_F e^2}{4\pi\epsilon_0\epsilon_r RT}\frac{d\kappa}{d\sqrt{I}} = \frac{N_A z'_M z'_F e^2}{4\pi\epsilon_0\epsilon_r RT}\sqrt{\frac{2000e^2N_A}{\epsilon_0\epsilon_r k_B T}} = Az'_M z'_F \tag{17}$$

Our experimental data for PI3K-SH3 and glucagon (Figure 4 in the main manuscript, individual values of ΔG^0can be found in tables 5 and 6 below) show that the slope is larger for PI3K-SH3, suggesting a higher effective charge that destabilizes the fibrils. This is consistent with the higher formal charge of PI3K-SH3 at this acidic pH, based on the amino acid sequence. In our analysis, we explored two different ways to fit the ionic strength dependence data, by keeping m fixed to the values determined previously and by fitting m globally to the ionic strength-dependent data set (see two columns in tables 5 and 6). We found that the general conclusions drawn here are independent of the exact manner in which the denaturation curves are fitted, and we show the results of the method with fixed m-value in the plots in the main manuscript.

We next proceed to relate the ionic strength dependencies of both kinetics and thermodynamics of fibril elongation. Our analysis above shows that the slopes for the kinetic and thermodynamic ionic strength dependencies are both independent of the characteristic distances, $r^{\ddagger}$ and r^{eq}, and

have the same numerical pre-factor, $A = \frac{N_A e^2}{4\pi\epsilon_0\epsilon_r RT}\sqrt{\frac{2000e^2N_A}{\epsilon_0\epsilon_r k_B T}}$. Therefore, in order to eliminate the numerical constant A, we can express the ratio of the slopes as:

$$\frac{d\log R}{d\sqrt{I}} \Big/ \frac{d\log K_e}{d\sqrt{I}} = \frac{z_M z_F}{z'_M z'_F} \tag{18}$$

We next perform a close analysis of the behavior of PI3K-SH3 for which both the dependence of the kinetics[15] and thermodynamics (this work) on solution ionic strength has been determined. We find that the slopes and therefore products of the effective charges are extremely similar in both the transition state and the final state (Figure 5 a of the main manuscript). This finding provides strong evidence for the fact that the transition state ensemble of fibril elongation, at least in this protein system, is highly product-like, regarding the center of mass distance component of the multi-dimensional reaction coordinate[16]. It is likely that under these conditions of high net charge, the electrostatic interactions are dominated by the center of mass distance between the newly incorporating monomer and the monomer that corresponds to the fibril end, rather than by the internal degrees of freedom. Therefore, no information on the similarity of the internal structures between transition state ensemble and final state can be obtained from our analysis.

References

[1] A. Fersht, *Structure and Mechanism in Protein Science*, W.H. Freeman, New York, 1999.

[2] T. Narimoto, K. Sakurai, A. Okamoto, E. Chatani, M. Hoshino, K. Hasegawa, H. Naiki and Y. Goto, *FEBS Letters*, 2004, **576**, 313–319.

[3] A. J. Baldwin, T. P. J. Knowles, G. G. Tartaglia, A. W. Fitzpatrick, G. L. Devlin, S. L. Shammas, C. A. Waudby, M. F. Mossuto, S. Meehan, S. L. Gras, J. Christodoulou, S. J. Anthony-Cahill, P. D. Barker, M. Vendruscolo and C. M. Dobson, *J Am Chem Soc*, 2011, **133**, 14160–14163.

[4] R. Porcari, C. Proukakis, C. A. Waudby, B. Bolognesi, P. P. Mangione, J. F. S. Paton, S. Mullin, L. D. Cabrita, A. Penco, A. Relini, G. Verona, M. Vendruscolo, M. Stoppini, G. G. Tartaglia, C. Camilloni, J. Christodoulou, A. H. V. Schapira and V. Bellotti, *J Biol Chem*, 2015, **290**, 2395–2404.

[5] F. Oosawa and M. Kasai, *J Mol Biol*, 1962, **4**, 10–21.

[6] F. Oosawa, *Thermodynamics of the Polymerization of Protein*, Academic Press Inc, 1975.

[7] D. Zhao and J. S. Moore, *Org. Biomol. Chem.*, 2003, **1**, 3471–3491.

[8] M. M. J. Smulders, M. M. L. Nieuwenhuizen, T. F. A. de Greef, P. van der Schoot, A. P. H. J. Schenning and E. W. Meijer, *Chemistry A European Journal*, 2010, **16**, 362–367.

[9] P. A. Korevaar, C. Schaefer, T. F. A. de Greef and E. W. Meijer, *JACS*, 2012, **134**, 13482–13491.

[10] J. Zurdo, J. I. Guijarro, J. L. Jimenez, H. R. Saibil and C. M. Dobson, *JMB*, 2001, **311**, 325–340.

[11] C. Boesch, A. Bundi, M. Oppliger and K. Wüthrich, *Eur J Biochem*, 1978, **91**, 209–214.

[12] A. K. Buell, *International Review of Cell and Molecular Biology*, 2017, **329**, 187–226.

[13] S. I. Cohen, R. Cukalevski, T. C. Michaels, A. Šarić, M. Törnquist, M. Vendruscolo, C. M. Dobson, A. K. Buell, T. P. Knowles and S. Linse, *Nature chemistry*, 2018, **10**, 523.

[14] P. Debye and E. Hückel, *Phys Zeitschr*, 1923, **24**, 185–206.

[15] A. K. Buell, P. Hung, X. Salvatella, M. E. Welland, C. M. Dobson and T. P. J. Knowles, *Biophys J*, 2013, **104**, 1116–1126.

[16] A. K. Buell, J. R. Blundell, C. M. Dobson, M. E. Welland, E. M. Terentjev and T. P. J. Knowles, *Phys Rev Lett*, 2010, **104**, 228101.

[17] T. C. Michaels, L. X. Liu, S. Curk, P. G. Bolhuis, A. Šarić and T. P. Knowles, *Molecular Physics*, 2018, **116**, 3055–3065.

[18] A. K. Buell, A. Dhulesia, D. A. White, T. P. J. Knowles, C. M. Dobson and M. E. Welland, *Angew Chem Int Ed Engl*, 2012, **51**, 5247–5251.

[19] W. K. Kegel and P. van der Schoot, *Biophys. J.*, 2004, **86**, 3905–3913.